Design Optimization of Bistable NES

Wu Zhenhang, Sébastien Seguy, Manuel Paredes

HAL Id: hal-03273272

https://hal.insa-toulouse.fr/hal-03273272

Submitted on 1 Jul 2021

Design Optimization of Bistable NES

Zhenhang Wu
Institut Clément Ader (ICA), CNRS, INSA-ISAE-Mines
Albi-UPS, Université de Toulouse,
3 rue Caroline Aigle,
Toulouse, 31400, France
e-mail: zhenhang.wu@insa-toulouse.

Sébastien Seguy
Institut Clément Ader (ICA), CNRS, INSA-ISAE-Mines
Albi-UPS, Université de Toulouse,
3 rue Caroline Aigle,
Toulouse, 31400, France
e-mail: sebastien.seguy@insa-toulouse.fr

Manuel Paredes
Institut Clément Ader (ICA), CNRS, INSA-ISAE-Mines Albi-UPS, Université de Toulouse,
3 rue Caroline Aigle,
Toulouse, 31400, France
e-mail: manuel.paredes@insa-toulouse.fr

Abstract—*This work mainly focuses on the optimization of the control strategy to obtain a bistable NES that achieves maximum efficiency under different harmonic excitations. As excitation increases, four unique regimes appear in turn. According to its distribution of characteristic responses regimes, the maximum efficiency point occurs when the Strongly Modulated Response (SMR) disappears. The optimal stiffness for a given excitation is expressed as a function of negative stiffness, which gives the possibility of controlling it by adjusting the pre-compressed length in a four spring system. The model of the device consists of 2 conical and 2 linear springs that counterbalance one another and provide the desired stiffness. The optimal absorbing range of the device is found by numerical investigation. The result of the primary static experiment proves that the model and stiffness control strategy are valid. This work offers some fundamental procedures for the optimal design of a bistable NES and paves the way for its practical implementation.*

Keywords— Bistable NES, Response regimes, Multiple Scales Method, Optimization, Stiffness control

I. INTRODUCTION

Harmful vibration can reduce the life of civil constructions and mechanical structures, and increase errors in manufacturing processes. Suppressing such undesirable vibration has become a long-standing issue. The traditional solution is to use Tuned Mass Damping (TMD) as a linear absorber. However, the capability of TMD is restricted to a narrow frequency band near its natural frequency. To overcome the drawbacks, the Nonlinear Energy Sink (NES) has been proposed and is becoming an active research field. It uses a relatively small attached mass, which is connected to the primary system by essentially cubic nonlinear stiffness and damping. The energy of Linear Oscillator (LO) is irreversibly transferred into the NES and dissipated by the damping. This Targeted Energy Transfer (TET) results from 1:1 transient resonance capture [1]. During the TET, intensive energy transfer leads to high efficiency in absorbing vibration. The efficiency with which this mechanism absorbs vibration has been explored by both numerical [2] and experimental methods [3].

A certain high energy threshold needs to be reached to activate intensive energy dissipation. With the introduction of negative linear stiffness in a cubic NES, a bistable NES can be set up, which also shows high efficiency in processing a low energy input because of nonlinear beating. In the cubic case, a small NES mass ratio and low damping are required to ensure the occurrence of TET. Increasing the nonlinear stiffness makes the system more suitable for handling low energy input, which is considered as its core property. In the bistable case, the diameter and depth of the potential well expand with a larger value of negative stiffness [4]. The bistable NES can be constructed by introducing negative stiffness between the primary system and the attached NES mass. This essentially changes the dynamic regimes. When negative stiffness is included in the nonlinear stiffness, the modified bistable NES can absorb input shock energy with high efficiency [5].

By considering the variety of nonlinearity, a number of novel NES are proposed and investigated, each with its own potential. They include vibro-impact NES, rotational NES [7], and piecewise NES. In these systems, the impact acceleration can be suppressed mostly by the enhanced single side vibro-impact NES. Because of the above characteristics, potential applications have included the control of seismic vibrations in built structures, flutter mitigation in a hypersonic 3-D wing and chatter control in a turning process [5].

However, the traditional NES is not reconfigurable, which restricts its general applications in various conditions. Numerous attempts have been made to overcome this drawback, for example, a time-varying inertial mass is provided to better absorb a large initial impulse and lower energy pumping threshold in [8]. The distance between the central magnetic mass and the fixed magnetic mass is shown to be easily controlled to build a tunable stiffness in [9]. These kinds of method provide great flexibility in the use of NES in different mechanical contexts

The paper is organized as follows. In section 2, various response regimes are distinguished and investigated by the Multiple Scales method and complex variables method. The existence of negative stiffness introduces essentially chaotic behaviours. Based on the distribution of regimes, the optimal stiffness is selected to absorb input energy with maximum efficiency. In the next section, a system combining four springs - two conical springs and two pre-compressed springs - is presented. Its range of absorbing capability is also investigated. A pre-compressed length control strategy is presented in the fourth section. A bistable NES system, used to verify the previously determined optimal stiffness experimentally, is presented in the fifth section. The last section mentions some noteworthy conclusions.
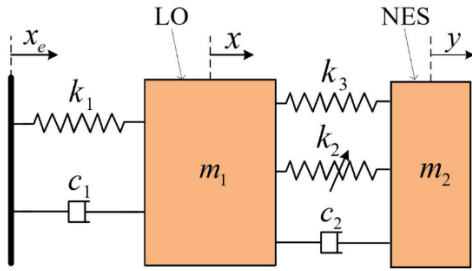
II. RESPONSE REGIMES UNDER HARMONIC EXCITATION

Figure 1   SCHEMATIC OF PRIMARY STRUCTURE (LO) AND NES

The proposed system is shown in Figure 1. m_1 and m_2 represent the mass of the Linear Oscillator (LO) and the NES. The LO is excited by the harmonic force x_e through the linear stiffness k_1 and damping c_1. The NES is attached to the LO by the cubic stiffness k_3, negative stiffness k_2, and damping c_2. The following equation governs the motion:

$$m_1\frac{d^2x}{dt^2}+c_1\frac{dx}{dt}+c_2\left(\frac{dx}{dt}-\frac{dy}{dt}\right)+k_1x+k_2\left(x-y\right)^3$$
$$+k_3\left(x-y\right)=k_1x_e+c_1\frac{dx_e}{dt} \tag{1}$$
$$m_2\frac{d^2y}{dt^2}+c_2\left(\frac{dy}{dt}-\frac{dx}{dt}\right)+k_2\left(y-x\right)^3+k_3\left(y-x\right)=0$$

The harmonic force is expressed as $x_e = G\ cos(\omega t)$. By substituting the variables as follows into Equation (1), the dimensionless form can be obtained.

$$\varepsilon=\frac{m_2}{m_1},\omega_0^2=\frac{k_1}{m_1},K=\frac{k_2}{m_2\omega_0^2},\delta=\frac{k_3}{m_2\omega_0^2},\lambda_1=\frac{c_1}{m_2\omega_0},$$
$$\lambda_2=\frac{c_2}{m_2\omega_0},\text{F}=\frac{G}{\varepsilon},\Omega=\frac{\omega}{\omega_0},\tau=\omega_0t \tag{2}$$

The new variables $v = x+\varepsilon y$, $w = x-y$ and the Manevitch complex variables $\varphi_1 e^{i\Omega\tau} = dv+i\Omega\tau v$, $\varphi_2 e^{i\Omega\tau} = dw+i\Omega\tau w$ are introduced into the dimensionless equation. Only terms containing $e^{i\Omega\tau}$ are conserved.

$$\dot{\varphi}_1+\frac{i\Omega}{2}\varphi_1+\frac{\varepsilon\lambda_1}{2(1+\varepsilon)}\left(\varphi_1+\varepsilon\varphi_2\right)-\frac{i\left(\varphi_1+\varepsilon\varphi_2\right)}{2\Omega(1+\varepsilon)}-\frac{\varepsilon F}{2}-\frac{i\varepsilon^2\lambda_1F\Omega}{2}=0$$

$$\dot{\varphi}_2+\frac{i\Omega}{2}\varphi_2+\frac{\varepsilon\lambda_1}{2(1+\varepsilon)}\left(\varphi_1+\varepsilon\varphi_2\right)-\frac{i\left(\varphi_1+\varepsilon\varphi_2\right)}{2\Omega(1+\varepsilon)}+\frac{\lambda_2\left(1+\varepsilon\right)}{2}\varphi_2 \tag{3}$$

$$-\frac{3iK\left(1+\varepsilon\right)}{8\Omega^3}\varphi_2^2\left|\varphi_2\right|-\frac{\varepsilon F}{2}-\frac{i\varphi_2\delta\left(1+\varepsilon\right)^2}{2\Omega}=0$$

The stable periodic solutions φ_{10} and φ_{20} can be obtained under the assumption that the derivative is zero. The multiple scales method, which can also be found in [10], is applied by substituting the following variables.

$$\frac{d}{d\tau}=\frac{\partial}{\partial\tau_0}+\varepsilon\frac{\partial}{\partial\tau_1}+\varepsilon^2\frac{\partial}{\partial\tau_2},\quad\varphi_i=\varphi_i(\tau_0,\tau_1,\tau_2),\quad\tau_k=\varepsilon^k\tau_0 \tag{4}$$

The terms that contain the coefficient of ε^0 give:

$$\frac{\partial}{\partial\tau_0}\varphi_2=0,$$
$$\frac{\partial}{\partial\tau_0}\varphi_2+\frac{\lambda_2}{2}\varphi_2+\frac{i}{2}\left(\varphi_2-\varphi_1\right)-\frac{3iK}{8}\varphi_2^2\left|\varphi_2\right|-\frac{1}{2}i\delta\varphi_2=0 \tag{5}$$

The new variables $\varphi_1(\tau_0)=N_1e^{i\theta 1}$, $\varphi_2(\tau_0)=N_2e^{i\theta 2}$ are introduced into Equation (5) to reveal the variation of the stable solution under the different levels of energy input.

$$Z_1=\lambda_2^2Z_2+\left(\delta-1\right)^2Z_2-\frac{3K}{2}\left(\delta-1\right)Z_2^2+\frac{9K^2}{16}Z_2^3, \tag{6}$$
$$Z_1=N_1^2,Z_2=N_2^2$$

The Slow Invariant Manifold (SIM) is an essential tool to describe the motion backbone with respect to the slow time scales. In the SIM structure, the two singular points Z_{21} and Z_{22} exist and divide the SIM into two stable branches and one unstable branch.

$$Z_{2i}=\frac{4\left(2(1-\delta)\mp\sqrt{\left(1-\delta\right)^2-3\lambda_2^2}\right)}{9K},i=1..2 \tag{7}$$

In the cubic case ($\delta=0$), the unstable region is considered as the possible reason for energy pumping and may give rise to the SMR.

III. BISTABLE NES RESPONSE REGIMES

The potential function of a bistable NES can divide the response regimes according to its energy level, where its potential function is defined as $U=\delta\ w^2/2+K\ w^4/4$. Obviously, the bistable NES has two equilibrium points, whose coordinates are ($\sqrt{-\delta/K}$,0) in Figure 2.
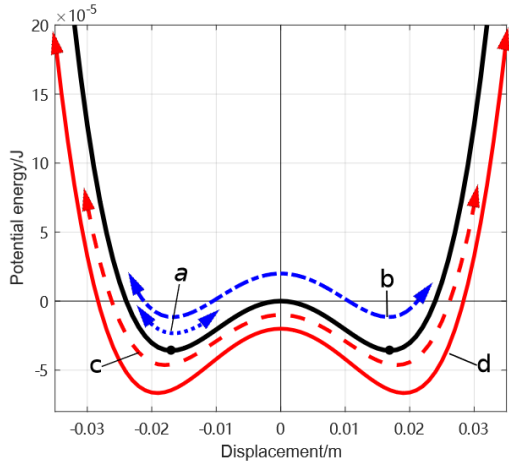
Figure 2   POTENTIAL FUNCTION OF THE UNPERTURBED SYSTEM:
(A) AN INTRA-WELL OSCILLATION; (B) CHAOTIC INTER-WELL
OSCILLATION; (C) STRONGLY MODULATED RESPONSE; (D)
STABLE PERIODIC RESPONSE

In different energy levels, four characteristic stages, which contain the time domain of w and v, and its phase trajectory in the SIM structure, are chosen and illustrated in Figure 3 with parameters $\varepsilon=0.01$, $\lambda_1=1.67$, $\lambda_2=0.167$, $K=1754$, $\delta=-0.44$. The four typical cases under the various G values: 0.08 mm, 0.15 mm 0.34 mm, and 0.45 mm respectively are chosen to show it dynamic behaviours in time domain in Figure 3.
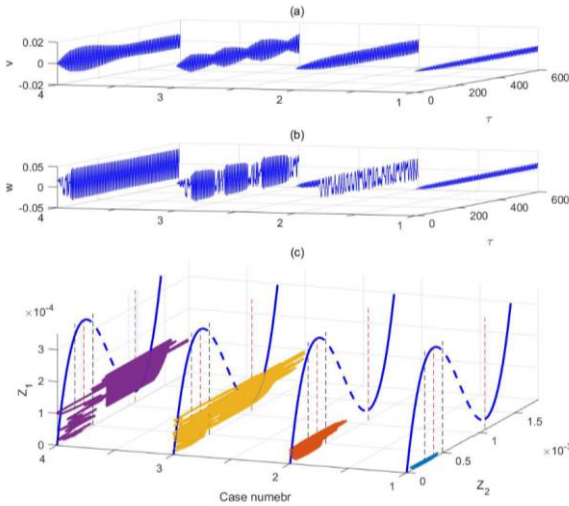

Figure 3   RESPONSE REGIMES IN BISTABLE NES (A) V
DISPLACEMENT (B) W DISPLACEMENT (C) PHASE TRAJECTORY
OF Z2 AND Z1

To better understand the efficiency distribution of a bistable NES over the different energy levels, the energy dissipated by a NES is defined in Equation (6) and its efficiency distribution is presented in Figure 4

$$E_{NES}(\tau) = \int_{\tau_0}^{\tau} \varepsilon\lambda_2 (\dot{x} - \dot{y})^2 \, d\tau$$

$$E_{LO}(\tau) = \int_{\tau_0}^{\tau} \varepsilon\lambda_1 \dot{x}^2 d\tau, \quad r_{NES} = \frac{100\% \times E_{NES}}{E_{LO} + E_{NES}}$$
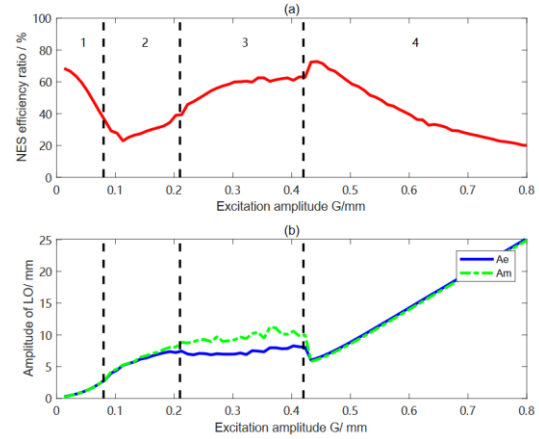
(8)

Figure 4   EFFICIENCY OF BISTABLE NES (A) THE MAXIMUM
AMPLITUDE (AM) AND MEAN AMPLITUDE (AE) OF LO FOR
DIFFERENT EXCITATIONS G (B) ENERGY DISSIPATION RATIO OF
BISTABLE NES.

According to the above 3 figures, to describe bistable NES behaviours under different amplitudes of excitation, four response regimes can be clearly identified:

(a) Intra-well oscillation

This period is a low energy motion. The displacement of the NES is restricted to one of the wells, in the vicinity of equilibrium (x_0, 0). Unlike the situation in the cubic case, the phase trajectory is not located in the left stable branch of the SIM and symmetrical with the attractor axis. The small amplitudes of w and v are considered as a nonlinear beat that helps the system achieve relatively high efficiency.

(b) Chaotic inter-well oscillation

With the increase in energy, the motion of the phase trajectory exceeds the pseudo-separatrix and crosses two wells, so chaos occurs. The chaos phenomenon is the characteristic motion of a bistable NES. The Melnikov method is employed to determine the boundary of the chaos response for the homoclinic bifurcation. The trajectory in the SIM structure (case 2 in subplot (c) of Figure 3) occupies a chaos region and will grow and expand without jumping. The system remains in a relatively low-efficiency level. The amplitude is an unstable result in that the maximum amplitude A_m and mean amplitude A_e start to separate. The chaotic inter-well oscillation period also involves other subharmonic oscillation, which is beyond the scope of our present considerations.

(c) Strongly modulated response

When its energy continues to grow, the system still shows the 'jumping' phenomenon. Initially, the phase trajectory is located in the chaos region and is expanding. Then the phase trajectory jumps to the right SIM branch and moves down along it. When it reaches the singular point, it will jump back to the chaos region and expand until the next

jumping cycle. Unlike the situation in the cubic NES case, the SMR is triggered by chaos expanding behaviours instead of the phase trajectory reaching its singular point Z_{21}. In this stage, the amplitude of LO increases when NES performs chaotic motion and declines when systems have 1:1 resonance, where the LO and NES oscillate at the same frequency. The amplitude of LO appears in an unstable stage. The distance between the A_e and A_m becomes constant, confirming that the SMR occupies the whole time if the excitation increases. Its efficiency achieves a relatively high level at this moment.

(d) Stable response

In a high energy level, the SIM continues to function and describes the stable response. Once the excitation is a little greater than G_{2c}, the SMR disappears and the system produces a stable response. It symbolizes the saturation of energy absorption in the bistable NES, which is similar to the cubic case. The maximum efficiency points occur in the transition between SMR and stable response period. According to [10], the excitation threshold G_{2c} can be considered as optimal excitation to deduce the optimal stiffness reversely. The maximum amplitude and mean amplitude of LO coalesce again.

$$G_{ic} = \varepsilon \frac{N_{2i}}{4} \frac{F_1}{F_2}, i = 1, 2$$

$$F_1 = 9K^2 N_{2,j}^2 \lambda_1 + 24K^2 N_{2,j}^2 \delta \lambda_1$$

$$-24KN_{2,j}^2 \lambda_1 + 16\delta^2 \lambda_1 + 16\lambda_1 \lambda_2^2 + 32\delta \lambda_1 + 16\lambda_1 + 16\lambda_2 \qquad (9)$$

$$F_2 = \sqrt{9K^2 N_{2,j}^4 + 24KN_{2,j}^2 \delta - 24KN_{2,j}^2 + 16\lambda_2^2 + 16\left(\delta^2 - 1\right)^2}$$

For a given excitation, G, there is an optimal stiffness to absorb energy at maximum efficiency. Substituting the G into the above equation and solving the optimal stiffness value, the optimal nonlinear stiffness to adapt to the given excitation is expressed as:

$$K_m = \frac{2}{81} (\varepsilon^2 (-144\delta \lambda_1^2 \lambda_2^4 + 72\delta^2 \lambda_1^2 \lambda_2^2 - 36\delta^3 \lambda_1 \lambda_2$$

$$-7272\delta \lambda_1^2 \lambda_2^2 - 324\delta \lambda_1 \lambda_2^3) + 1086\delta^2 \lambda_1 \lambda_2 - 108\delta \lambda_1 \lambda_2$$

$$-24\delta^3 \lambda_1^2 \lambda_2^2 + 48\mu \delta \lambda_1^2 + 108\mu \lambda_1 \lambda_2^3 - 12\mu \delta^4 \lambda_1^2$$

$$-36\mu \lambda_1 \lambda_2 + 48\mu \delta^3 \lambda_1^2 - 24\mu \lambda_1^2 \lambda_2^2 - 72\mu \delta^2 \lambda_1^2$$

$$-8\delta^2 \lambda_1^2 + 40\delta^4 \lambda_1^2 + 144\lambda_1^2 \lambda_2^4 - 80\delta^3 \lambda_1^2 \qquad (10)$$

$$+80\delta^2 \lambda_1^2 + 24\lambda_1^2 \lambda_2^2 + 324\lambda_1 \lambda_2^3 - 40\delta \lambda_1^2 - 162\delta \lambda_2^2$$

$$+36\lambda_1 \lambda_2 + 8\lambda_1^2 + 36\mu \lambda_1^2 \lambda_2^4 + 162\lambda_2^2 - 12\mu \lambda_1^2 + 81\mu \lambda_2^2$$

$$+72\mu \delta \lambda_1 \lambda_2 + 4\mu^3 \delta^2 \lambda_1^2 - 8\mu^3 \delta \lambda_1^2)^2 / (G^2 (\delta^2 + \delta \mu$$

$$+3\lambda_2^2 - 2\delta - \mu + 1))$$

$$\mu^2 = \delta^2 - 3\lambda_2^2 - 2\delta + 1$$

In the aim of finding the exact optimal stiffness under the given fixed excitation and comparing it with the optimal

stiffness expression, the different nonlinear stiffnesses, *K*, were fully tested and the result is presented in Figure 5.
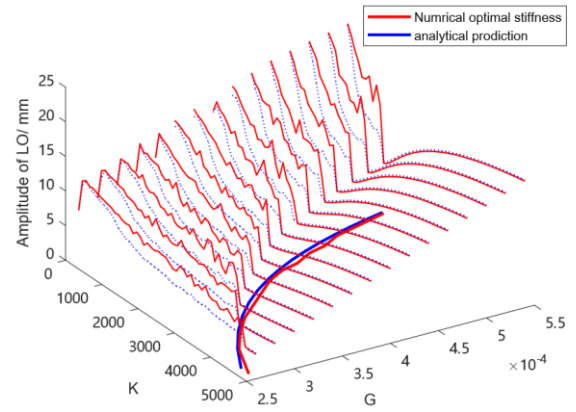

Figure 5   EFFICIENCY OF BISTABLE NES FOR DIFFERENT EXCITATIONS, G, WHERE THE NONLINEAR STIFFNESS, K, IS A CONTROL PARAMETER (ε=0.01, λ1=1.67, λ2=0.167 δ=−0.44)

The bold red line is the minimum amplitude of the projection of LO in the *K-G* plane, while the bold blue line is the analytical prediction of the optimal *K* value. Red line is A_m. Blue dotted line is A_e. An obvious tendency is observed: larger imposed force (input energy) leads to a smaller designed nonlinear stiffness for a fixed negative stiffness value. When the designed value nears the optimal value for a given excitation, the amplitude of LO will decline sharply. If the design stiffness is a little greater than the optimal value, it can still reduce the amplitude of the primary system with high efficiency. In a larger range, the analytical prediction can still describe the optimal $K-G$ curve well.

IV.   NUMERICAL VALIDATION OF FOUR SPRING SYSTEM

The transition from cubic NES to bistable NES is mainly controlled by the introduction of negative stiffness. And the negative stiffness k_3 and nonlinear stiffness k_2 both determine the optimal excitation. To control the stiffness and adapt to different energy input levels, a system combining four springs was constructed and is illustrated in Figure 6.
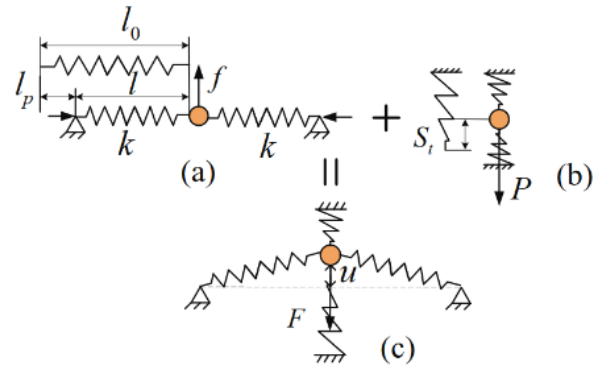

Figure 6   DETAILED DIAGRAM OF NES SYSTEM: (A) NEGATIVE STIFFNESS MECHANISM; (B) CONICAL SPRING; (C) THE COMBINING SYSTEM

The core component is the conical spring, which has two characteristic phases during the compression: (1) a linear phase and (2) a nonlinear phase. So the system consists of two conical springs, which are pre-compressed at the transition point to counterbalance the linear phase. The two linear springs are installed vertically with the nonlinear spring at a chosen pre-compressed length l_p in order to counterbalance the linear stiffness in the nonlinear phase and create the pure cubic or bistable NES. Its force-displacement relationship can be expressed as follows.

$$F = \left(a_1 + k_0 - 2k_l \frac{l_p}{l_{0l} + 2l_c - l_p} \right) u + \left(a_3 + k_l \frac{l_{0l} + 2l_c}{\left(l_{0l} + 2l_c - l_p \right)^3} \right) u^3 \quad (7)$$

where k_0 is the linear phase stiffness and a_1, a_3 are the linear stiffness and cubic stiffness in the nonlinear phase of a conical spring. l_{0l} and l_c are the lengths of the linear spring and connector, respectively. k_l is the stiffness of the linear spring. The optimal stiffness is a function of δ and, theoretically, the K can be detuned to meet the best tuned stiffness. By adjusting the pre-compressed length l_p, the system can process different negative stiffnesses k_3 and nonlinear stiffnesses k_2 to shift between the cubic NES and the bistable NES. So the system can adapt to various amplitudes with maximum efficiency in different contexts. The parameters of the system are presented as

	k_0	a_1	a_3	k_l
Value	187 N/m	280 N/m	4e5 N/m³	1060 N/m
	l_{0l}	l_c	l_p	
	50 mm	14.5 mm	14.3 mm	

TABLE 1   PARAMETERS OF FOUR SPRING SYSTEM

The blue trajectory in Figure 7 projects onto the K-δ plane as the values of K and δ of the systems vary with changing l_p. Obviously, the initial increase in pre-compression augments the values of both K and δ. The surface in Figure 7 is the corresponding target excitation that the system can sustain at maximum efficiency under different combinations of K and δ values.
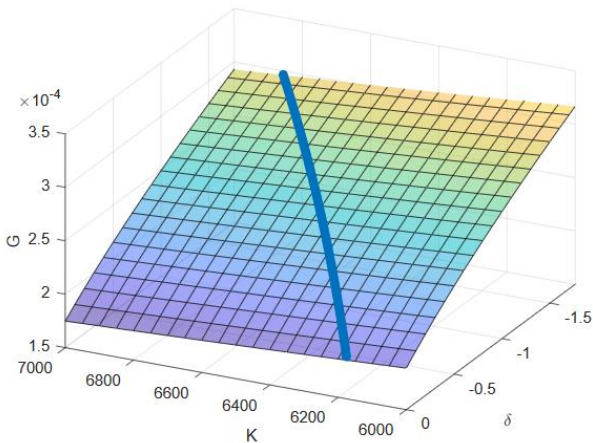
As the value of nonlinear stiffness and negative stiffness augments, according to Equation (9), the threshold excitation value, G_{2c}, increases, meaning that the bistable NES can sustain more intense excitation. In the fixed nonlinear stiffness condition, a variation in δ results in a more intense change in G than in the changed K and fixed δ condition. This phenomenon indicates that the more efficient method to adapt to different amplitude excitations is to adjust the δ value. Through the method of adjusting the pre-compressed length, the target excitation that bistable NES can absorb in maximum efficiency can be modulated.

In our numerical study, the length of pre-compression varies from 14.3 mm to 19 mm, so the NES system changes from a cubic NES to a bistable NES. The intervals of K and δ are [6179, 6855] and [0, -1.74] respectively. From Figure 7, the minimum optimal excitation is $G = 0.188$ mm and the maximum optimal excitation G is 0.3 mm. For our device, increasing l_p can enable the bistable system to sustain a larger excitation amplitude in maximum efficiency.

V.   PRELIMINARY STIFFNESS CONTROL EXPERIMENT

In order to verify the stiffness control method, the system of four combined springs was built (Figure 8) and its characteristic displacement force curve was tested.
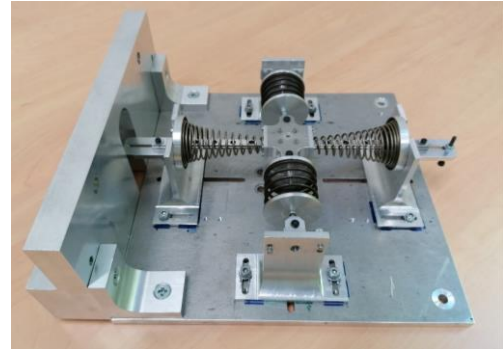

Figure 8   EXPERIMENT DEVICE

Figure 9 shows the difference between the target stiffness curve (solid line) and the actual result of the experiment (dashed dotted line). The pre-compressed lengths of cases 1, 2, and 3 were 16 mm, 18 mm, and 20 mm, respectively. In every case, the theoretical result described the experimental result with sufficient accuracy. The figure shows that two equilibria ($F = 0$) formed, one on either side of the displacement, which characterizes a bistable NES. The distance between the equilibrium points becomes greater when the l_p increases, resulting in the augmentation of the span and depth of the potential well. So it can be concluded that the control strategy of changing the length of pre-compression is feasible to produce desirable stiffness characteristics.
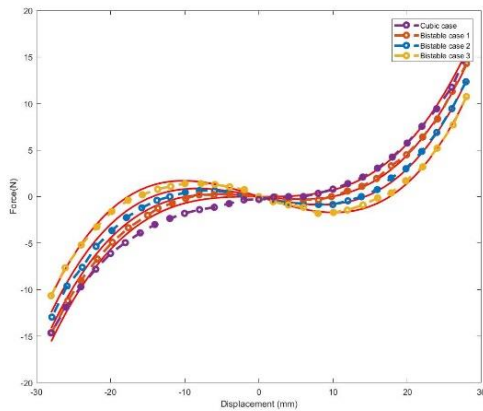
Figure 9   COMPARISON OF TARGET CURVE AND EXPERIMENTAL RESULT OF STATIC DISPLACEMENT FORCE CHARACTERISTIC OF DIFFERENT PRE-COMPRESSED LENGTH CASES

VI.   CONCLUSION

The current study investigates the optimal state of bistable NES based on the response regimes. The optimal point is selected from the standpoint of energy absorption efficiency. The numerical method indicates the feasibility of the control strategy and the primary stiffness control experiment is carried out. Several main conclusions can be drawn:

(1) With increasing harmonic amplitude excitation, the intra-well oscillation, chaotic inter-well oscillation, strongly modulated response and stable response occur in that order. The optimal point occurs in the transition period from SMR to stable response.

(2) In large amplitude energy input conditions, the threshold excitation G_{2c} calculated by the multiple scales method and complex variables method can represent the target excitation. Explained by the SIM structure, the singular point Z_{22} represents the point where this system reaches the maximum efficiency it can.

(3) For a given excitation, the optimal nonlinear stiffness value is reached by adjusting the pre-compressed length l_p. Larger l_p leads to increasing K and δ values. So the bistable NES system can sustain a larger amplitude excitation. The numerical simulation reveals that a slightly larger design value of nonlinear stiffness K can still lead to high efficiency in absorbing certain excitations.

(4) The experimental set-up is being built and the fundamental stiffness control has been carried out to meet the target stiffness with sufficient accuracy. Good agreement is observed between the theoretical and the experimental results.

VII.   REFERENCES

[1]   Kerschen, G, Lee, Y. S, Vakakis, A. F, McFarland, D. M., and Bergman, L. A. "Irreversible passive energy transfer in coupled oscillators with essential nonlinearity", Appl Math, Cambridge University Press, 66(2), 2005, pp. 648–679

[2]   Vaurigaud, B., Savadkoohi, A. T., and Lamarque, C.-H. "Targeted energy transfer with parallel non-linear energy sinks. Part i: design theory and numerical results". Nonlinear dyn, Springer, 66(4), 2011. pp. 763–780

[3]   McFarland, D. M, Kerschen, G, Kowtko, J. J, Lee, Y. S, Bergman, L. A, and Vakakis, A. F. "Experimental investigation of targeted energy transfers in strongly and nonlinearly coupled oscillators". J. AcoustSoc Am, Acoustical Society of America, 118(2), 2005, pp. 791–799.

[4]   Romeo F, Sigalov G, Bergman L A, et al. "Dynamics of a linear oscillator coupled to a bistable light attachment: numerical study", J. Comput. Nonlinear Dyn, ASME, 10(1), 2015, p. 011007

[5]   AL-Shudeifat, M. A. "Highly efficient nonlinear energy sink", Nonlinear Dyn, Springer, 76(4), 2014, pp. 1905–1920.

[6]   Sigalov, G., et al. "Resonance captures and targeted energy transfers in an inertially-coupled rotational nonlinear energy sink." Nonlinear dynamics, Springer, 69(4), 2012, pp. 1693-1704.

[7]   Gourc E, Seguy S, Michon G, et al. "Chatter control in turning process with a nonlinear energy sink", Adv Mat Res, Trans Tech Publications Ltd, 698: 2013, pp. 89-98.

[8]   Yang T, Hou S, Qin Z H, et al. "A dynamic reconfigurable nonlinear energy sink", J. Sound Vib, Elsevier, 494, 2020, p. 115629.

[9]   Benacchio S, Malher A, Boisson J, et al. "Design of a magnetic vibration absorber with tunable stiffness" Nonlinear Dyn, 85(2), 2016, pp. 893-911.

[10]   Manevitch, L. "The description of localized nor-mal modes in a chain of nonlinear coupled oscillators using complex variables". Nonlinear Dyn, Springer, 25(1-3) , 2001, pp. 95–109

[11]   Qiu, D., Li, T., Seguy, S., and Paredes, M. "Efficient targeted energy transfer of bistable nonlinear energy sink: application to optimal design", Nonlinear Dyn, Springer, 92(2), 2018, pp. 443–461.